Ion-beam-induced amorphization and order-disorder transition in the murataite structure

Jie Lian, L. M. Wang, and Rodney C. Ewing[a)]
Department of Geological Sciences, Department of Nuclear Engineering and Radiological Sciences, and Department of Materials Science and Engineering, University of Michigan, Ann Arbor, Michigan 48109

Sergey V. Yudintsev
Institute of Geology of Ore Deposits, Russian Academy of Sciences (RAS), Staromonetnii Pereulok 35, Moscow 109017, Russia

Sergey V. Stefanovsky
Schneizerischer Ingenieur-und Architektenverein (SIA) Radon, 7th Rostovskii Pereulok 2/14, Moscow 119121, Russia

(Received 17 February 2005; accepted 13 April 2005; published online 6 June 2005)

Murataite ($A_3B_6C_2O_{22-x/2}, F\bar{4}3m$), a derivative of an anion-deficient fluorite structure, has been synthesized as different polytypes as a result of cation ordering. Ion-beam-induced amorphization has been investigated by 1-MeV Kr^{2+} ion irradiation with *in situ* transmission electron microscopy. The critical amorphization dose was determined as a function of temperature and the degree of structural disordering. A lower critical amorphization temperature (~860 K) was obtained for the disordered murataite as compared with that of the murataite superstructure (930 to 1060 K). An ion-beam-induced ordered murataite to a disordered fluorite transition occurred in the murataite superstructure, similar to that observed in the closely related pyrochlore structure-type, $A_2B_2O_7$. The ion-beam-induced defect fluorite structure is more energetically stable in the murataite structure with a higher degree of structural disordering, as compared with the murataite superstructure. This suggests that the degree of intrinsic structural disorder has a significant effect on the energetics of structural disordering process; this affects the tendency toward the order-disorder structural transition for fluorite-related compounds and their response to ion-beam-induced amorphization.
 [DOI: 10.1063/1.1926394]

I. INTRODUCTION

Some anion-deficient defect fluorite structures are oxygen ion conductors with important potential applications as components in solid oxide fuel cells,[1–3] oxygen sensors,[4,5] oxygen pumps,[6] and catalysts.[7–9] The anion mobility, and hence the ionic conductivity, are strongly dependent on the extent of disordering of the oxygen vacancies and the interaction of mobile species with the cations. In the most commonly studied ionic conductor, yttrium-stabilized zirconia (YSZ), the ionic conductivity increases with the addition of Y due to the increasing oxygen-vacancy concentration. The charge-compensating oxygen vacancies caused by Y doping are preferentially located next to Zr^{4+}, leaving Y in an eightfold oxygen coordination.[10] However, the addition of Y dopant above 8 mol % results in a decrease in conductivity due to a significant association between oxygen vacancies and cations, reducing the concentration of the mobile oxygen vacancies available for migration.[11] Continuously increasing the amount of dopant (e.g., Y or lanthanides) in zirconia causes a structural transition from an anion-deficient fluorite structure to an ordered pyrochlore structure, e.g., $Gd_2Zr_2O_7$, where both the cations and the oxygen vacancies are ordered.[12] In this case, the structure becomes an ionic insulator.[13] One way to enhance the ionic conductivity is to induce structural disordering or dissociate vacancy-cation interactions at a high temperature, allowing the oxygen vacancies to migrate freely.[14,15] Ion-beam implantation (irradiation) has been used to modify the physical properties of pyrochlores by manipulating the microstructure and the degree of structural disordering in both cation and anion sublattices.[16,17] An ion-beam-induced order-disorder structural transformation occurs in pyrochlore compounds, and this structural transition has an important effect on the response of the pyrochlore structure to ion irradiation-induced amorphization,[18] as well as its electronic properties. The ion-beam-induced structural disordering is highly composition dependent, and pyrochlore compositions enriched in Zr show a greater tendency toward the order-disorder structural transition upon ion irradiation.[19] Preexisting structural disorder has been reported to have a significant effect on the ion-beam-induced amorphization in $MnNbTaO_6$ natural columbites, where the compounds having a higher-order parameter are less sensitive to the ion-beam-induced crystalline-to-amorphous transition than their partially ordered or disordered counterparts.[20] Very few studies have been conducted to investigate the influence of the extent of intrinsic structural disorder in fluorite-related phases (e.g., pyrochlores) on the order-disorder structural transformation and the susceptibility to ion-beam-induced amorphization. In this study, we

[a)]Electronic mail: rodewing@umich.edu

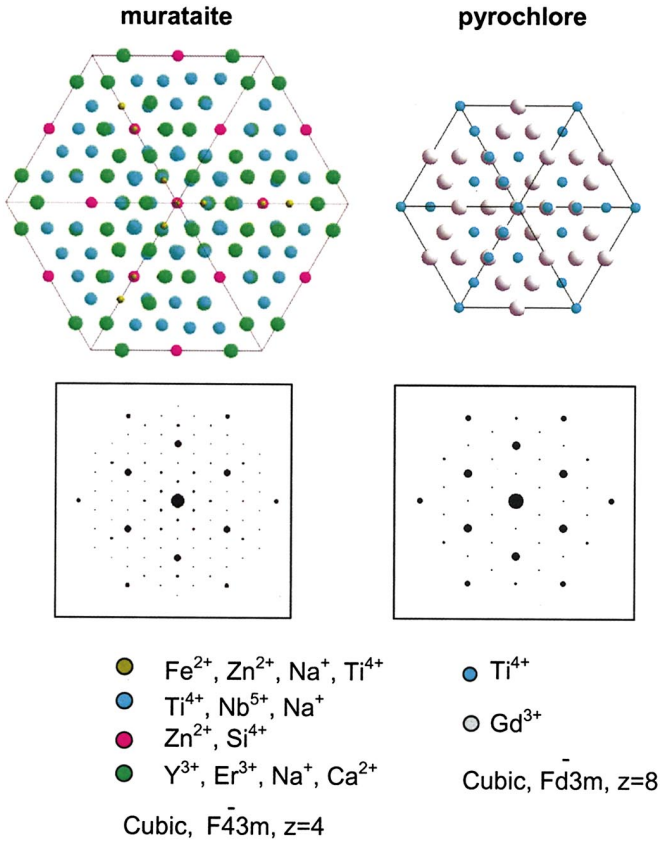

FIG. 1. Crystal structure along [111] zone axis and calculated diffraction patterns showing the superstructure of fluorite unit cells for muratatite ($3\times3\times3$) and pyrochlore ($2\times2\times2$). The diffraction subset with a high intensity corresponds to the basic fluorite unit cell.

have synthesized muratatite polytypes, anion-deficient fluorite-structured oxides, and investigated the effects of different degrees of structural disordering on ion-beam-induced amorphization and the order-disorder structural transition.

II. EXPERIMENT

A. Material synthesis and characterization

Muratatite ($F\bar{4}3m, a=1.488$ nm, $Z=4$) is an isometric derivative of the fluorite structure (Fig. 1). The general formula of synthetic muratatite is $A_3B_6C_2O_{22-x/2}$, where the eight-coordinated A sites are occupied by large Na^+, Ca^{2+}, REE^{3+}, and $An^{3+/4+}$ cations; six-coordinated B sites, small Ti^{4+}, Fe^{3+}, and Al^{3+}; four- and five-coordinated C sites, $Mn^{2+/3+}$, Fe^{3+}, and Zn^{2+}.[21–26] Three samples of muratatite ceramics in the system of Ca–Ti–U–Mn–Al–Fe–Zr–Ce–O were prepared by sintering at 1400–1600 °C followed by crystallization under slightly oxidizing conditions (in air). Two of the samples ($M1/7$ and $M3/7$) were produced in platinum crucibles in a resistive furnace, and the third sample was obtained by the inductive melting in a cold crucible (IMCC). The phases in the sintered ceramics were identified by the x-ray diffraction, and the chemical compositions (Table I) were determined by energy dispersive spectroscopy (EDS) using scanning electron microscopy (SEM) and transmission electron microscopy (TEM). Depending on the conditions of synthesis, the cations order onto specific sites that lead to an ordered muratatite superstructure, for which the unit-cell edge is a multiple of the fluorite unit-cell edge. Muratatite can occur as a superstructure of three multiples of the fluorite unit cell (Mu-$3\times3\times3$), five multiples (Mu-$5\times5\times5$) and eight multiples (Mu-$8\times8\times8$), as shown in Fig. 2. The unit-cell parameters for muratatite polytype with three, five, and eight multiples are ~1.48, ~2.46, and ~3.94 nm, respectively. The diffraction pattern (see Fig. 1), calculated using the CRYSTALKIT software based on the structural model of natural muratatite ($F\bar{4}3m, a=1.488$ nm, $Z=4$), is identical to that of the synthetic Mu-$3\times3\times3$ diffraction pattern [Fig. 2(b)], suggesting that the muratatite (Mu-$3\times3\times3$) is essentially a fluorite structure-type with a triple arrangement of the fluorite unit cell containing oxygen and metal vacancies. The strong diffraction maxima correspond to the underlying fluorite unit cell, and the satellite spots in the diffraction pattern from Mu-$3\times3\times3$ [Fig. 2(b)] are the result of cations with different scattering powers ordered on specific sites in the muratatite structure. In addition to the strong subset of fluorite diffraction maxima, the long-range ordering resulting from commensurate modulation can be observed in the muratatite structure, as manifested by the satellite spots of $G_F\pm1/5\langle111\rangle^*$ and $G_F\pm1/8\langle111\rangle^*$ in Figs. 2(c) and 2(d), respectively. These satellite spots are characteristic of the periodic perturbations of the fluorite unit cell. Incommensu-

TABLE I. Chemical compositions (wt %) of samples and individual phases determined by EDS measurements. The estimated amounts of individual phases in the synthetic ceramics are given as vol % in parenthesis.

Sample		CaO	MnO	Ce_2O_3	UO_2	ZrO_2	Al_2O_3	TiO_2	FeO	Minor phases
IMCC	Bulk	10.0	10.0	···	10.0	5.0	5.0	55.0	5.0	rutile (5%)
	Mu-$5\times5\times5$ (60%)	11.5	9.1	···	12.0	8.3	3.7	50.7	4.7	crichtonite (5%)
	Mu-$3\times3\times3$ (25%)	9.4	11.9	···	5.3	3.0	9.3	52.8	8.3	glass (5%)
$M1/7$	Bulk	10.0	10.0	···	10.0	5.0	5.0	55.0	5.0	rutile (10%)
	Mu-$5\times5\times5$ (70%)	12.2	9.3	···	9.7	5.8	4.4	51.1	4.5	
	Mu-$8\times8\times8$ (20%)	10.9	12.2	···	8.1	2.8	6.1	53.3	6.7	
$M3/7$	Bulk	8.0	8.0	20.0	8.0	4.0	4.0	44.0	4.0	crichtonite (10%)
	pyrochlore (65%)	8.9	5.1	27.7	10.5	4.5	0.9	39.6	1.0	
	disordered muratatite (25%)	8.5	10.7	11.3	2.7	1.6	7.8	48.5	7.1	

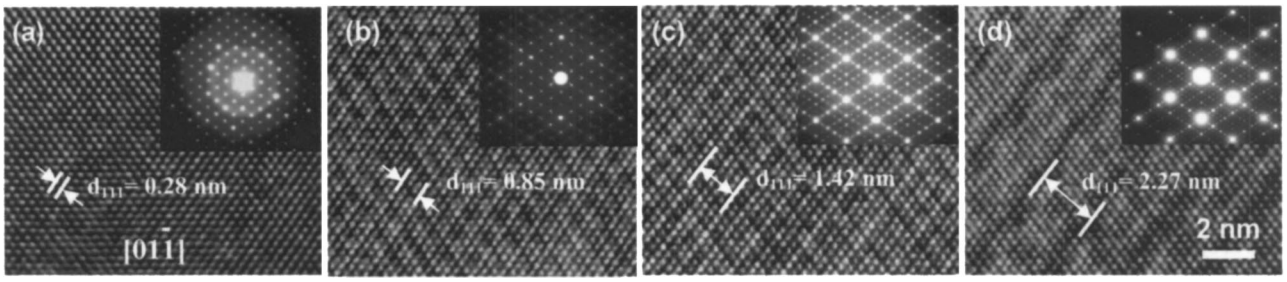

FIG. 2. HRTEM images and selected-area electron diffraction (SAED) patterns showing structural ordering in muratite: (a) a disordered muratite, (b) three multiples of the fluorite unit cell (Mu-$3\times3\times3$), (c) five multiples of the fluorite unit cell (Mu-$5\times5\times5$), and (d) eight multiples of the fluorite unit cell (Mu-$8\times8\times8$).

rate composition modulations also occur in the muratite superstructure, as revealed by the unequal spacing of the satellite diffraction maxima of the 2/5 and 3/5 $\langle111\rangle^*$ and 3/8 and the 5/8 $\langle111\rangle^*$ in Mu-$5\times5\times5$ and Mu-$8\times8\times8$, respectively, which have a stronger contrast than the weaker satellite diffraction maxima resulting from long-range ordering. A disordered muratite structure also was synthesized in which the cell dimension is almost identical to that of the three-multiple structure; however, the loss of long-range order is evident as revealed by the disappearance of the weak satellite diffraction maxima in the selected-area electron diffraction (SAED) pattern [Fig. 2(a)]. Incommensurately modulated structures in complex ceramics can result from atomic ordering on crystallographically equivalent sites, from atomic positional displacement, or from both structural distortions and fluctuations in composition.[27] Chemical analyses by EDS indicated very complex compositions for these synthetic muratite-type ceramics (Table I). In both natural and synthetic muratite structures, isomorphic cation exchange influences the compositional modulations. Cation substitutions typically occur at the *A* site: $Ca^{2+}=Mn^{2+}$, $2Ca^{2+}=Na^{+}+REE^{3+}$; *B* site: $Ti^{4+}=Zr^{4+}=U^{4+}$, $Zn^{2+}=Fe^{2+}$; *C* site: $2Ti^{4+}=(Al,Fe)^{3+}+Nb^{5+}$; coupled *A* and *C* site substitutions: $Ca^{2+}+Ti^{4+}=Na^{+}+Nb^{5+}$, $Ca^{2+}+Ti^{4+}=REE^{3+}+(Al,Fe)^{3+}$, $Ca^{2+}+2Ti^{4+}=Ce^{4+}+2(Al,Fe)^{3+}$. Due to the complex and extensive cation substitutions, it is difficult to decipher the nature of chemical composition modulation in muratite structure. Karimova *et al.*[26] indicated that the atoms with strong scattering properties are located at the planes that intercept at 1/3 of the distance of the diagonal of the large Mu-$5\times5\times5$ or Mu-$8\times8\times8$ unit cell perpendicular to [111] direction. This displacement causes the incommensurate modulations corresponding to the satellite maxima at 3/5 and 3/8 $\langle111\rangle^*$, respectively. The satellite diffraction spot at 2/5 $\langle111\rangle^*$ in the SAED pattern from Mu-$5\times5\times5$ is the satellite reflection of the $\langle111\rangle$ diffraction maxima. Similarly, the satellite diffraction spot at 5/8 $\langle111\rangle^*$ is a satellite reflection of the $\langle111\rangle$ diffraction maxima in the SAED pattern for Mu-$8\times8\times8$. The ordered muratite superstructure is closely related to pyrochlore, which contains eight fluorite unit cells as the unit-cell edge has doubled ($2\times2\times2$) (Fig. 1). These multiple superstructures provide an unusual opportunity to investigate the effect of the structural disordering on the order-disorder structural transition and the response of fluorite-related compounds to ion-beam-induced amorphization.

B. Ion irradiation and *in situ* TEM observation

A 1-MeV Kr^{2+} ion irradiation was performed over the temperature range of 293 to 1073 K using IVEM-Tandem facility at Argonne National Laboratory, and the ion flux was 1.25×10^{12} ions/cm^2/s. Prethinned plain-view TEM samples used for ion irradiations were prepared by mechanical polishing followed by 4-keV Ar^+ ion milling. Based on SRIM 2000 code calculation, the ion range ($\sim$300 nm) of 1-MeV Kr^{2+} is greater than the typical sample thickness ($\sim$200 nm) suitable for a TEM observation. Most of 1 -MeV Kr^{2+} ions, therefore, pass through the sample thickness examined, and ion-implantation effects are negligible. During irradiation, the ion beam was aligned approximately normal to the sample surface. To avoid concurrent electron-beam irradiation damage, the electron beam was turned off during ion irradiation. The crystalline-to-amorphous transformation was monitored intermittently by observing the SAED patterns. Ion irradiation combined with *in situ* TEM allowed us to follow the evolution of the microstructure with increasing ion fluence at the atomic scale in real time. The critical amorphization fluence F_c was determined as the fluence at which all of the diffraction maxima in the SAED pattern had disappeared. The critical amorphization fluence has been converted to displacements per atom (dpa) using the SRIM2000 simulation. No threshold displacement energies for the atoms in the muratite structure are available. Thus, in order to make a comparison with pyrochlore compositions, a threshold displacement energy of 50 eV was used for SRIM calculations of the muratite structure. Microstructural evolution upon ion irradiation was determined by *ex situ* high-resolution TEM (HRTEM) using JEOL 2010 F with a field-emission source.

III. RESULTS AND DISCUSSION

A. Ion-beam-induced amorphization and temperature dependence

The muratite ceramic was readily amorphized by ion-beam irradiation at room temperature. The characteristic microstructural evolution due to increasing levels of radiation damage (i.e., the gradually decreasing intensity of the diffraction maxima and the appearance of a diffuse scattering

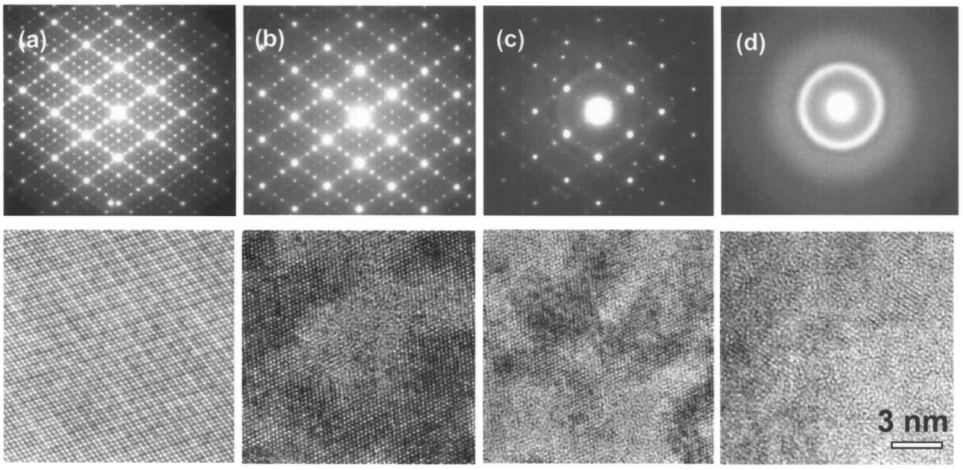

FIG. 3. SAED patterns and corresponding HRTEM images showing the susceptibility of the five-multiple murataite in sample $M1/7$ subjected to ion-beam irradiation at room temperature: (a) original, (b) 4.38×10^{13} (0.035 dpa), (c) 9.39×10^{13} (0.075 dpa), and (d) 15.6×10^{13} ions/cm^2 (0.125 dpa).

halo with increasing ion dose) was observed by *in situ* TEM (Fig. 3). Above the critical amorphization dose, diffraction maxima from the crystalline domains disappear completely, and the final, fully amorphous state was achieved at a relatively low dose, e.g., ~0.125 dpa (1.56×10^{14} ions/cm^2) for Mu-$5\times5\times5$ in the $M1/7$ sample at room temperature (Fig. 3). The critical amorphization dose increased with the increasing irradiation temperature due to dynamic annealing. The temperature dependence of amorphization is a result of the competition between damage production and recovery processes. Based on a cascade-quenching model,[28] the critical amorphization temperatures T_c of murataite ceramics subjected to 1-MeV Kr^{2+} ion irradiations can be determined by fitting the experimental data (Figs. 4 and 5) using a temperature-dependent amorphization dose function (for details, see Ref. 28). The critical amorphization temperatures are ~930 and 1030 K for Mu-$5\times5\times5$ and Mu-$8\times8\times8$ murataite polytypes in the $M1/7$ sample, respectively. Limited data were obtained for Mu-$3\times3\times3$ in the IMCC sample during the ion irradiation process. The data points of Mu-$3\times3\times3$ were plotted in the temperature-dependence curve with the data of Mu-$5\times5\times5$ in the IMCC sample (Fig. 4). The critical amorphization temperature is estimated to be ~1060 K for Mu-$5\times5\times5$ in the IMCC sample. The critical amorphization temperature for Mu-$3\times3\times3$ polytype may be slightly lower than that of Mu-$5\times5\times5$ in the IMCC sample, based on the fact that the available critical amorphization dose of Mu-$3\times3\times3$ are slightly higher as compared with that of Mu-$5\times5\times5$ in the IMCC sample at the same irradiation conditions. The discrepancy in the critical temperature for Mu-$5\times5\times5$ phases in $M1/7$ and IMCC could be due to their slightly different chemical compositions and thermal history at different synthetic conditions. A lower critical amorphization temperature (~860 K) was obtained for the disordered murataite phase with the loss of the long-range order (Fig. 5) in the sample $M3/7$. The radiation response of a structurally related pyrochlore, a $2\times2\times2$ polytype, in the $M3/7$ sample was also studied, and the critical amorphization temperature with 1-MeV Kr^{2+} ion irradiation was ~1010 K. These results suggest a decreased susceptibility to ion-beam irradiation-induced amorphization for the disordered murataite, as evidenced by the relatively lower critical amorphization temperatures above which full amorphization cannot be achieved, as compared with that of the ordered murataite and pyrochlore structures.

B. Ion-beam-induced order-disorder structural transition

Similar to the ion irradiated pyrochlore structures,[29] all of the irradiated murataite structure-types displayed an ion irradiation-induced murataite-to-defect-fluorite structural transformation. The diffraction maxima from the superstruc-

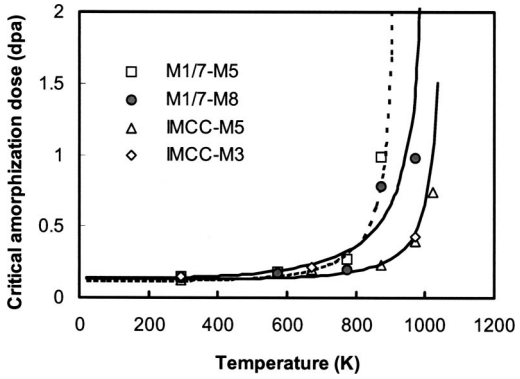

FIG. 4. Temperature dependence of the critical amorphization dose of murataites in samples $M1/7$ and IMCC with 1-MeV Kr^{2+} irradiation.

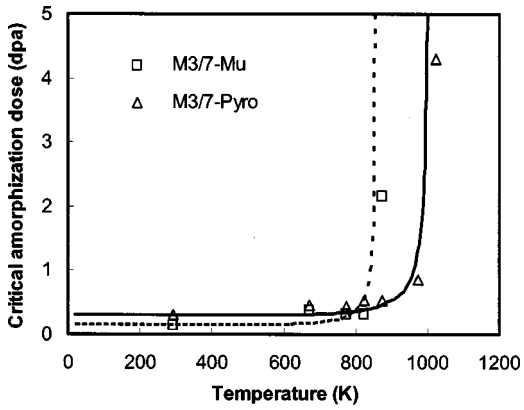

FIG. 5. Temperature dependence of the critical amorphization dose of the disordered murataite and ordered pyrochlore in $M3/7$ with 1-MeV Kr^{2+} irradiation.

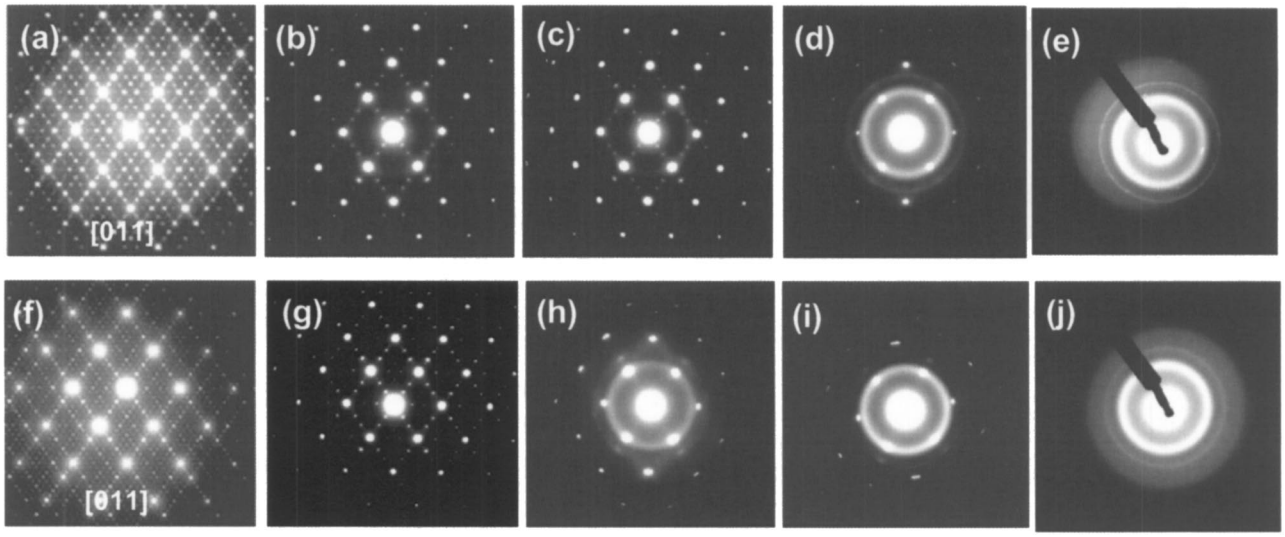

FIG. 6. Upper row: a sequence of SAED patterns of Mu-$5\times5\times5$ ($M1/7$) subjected to 1-MeV Kr^{2+} ion irradiation at 873 K: (a) original, (b) 3.125×10^{14} (0.25 dpa), (c) 5.625×10^{14} (0.45 dpa), (d) 7.5×10^{14} (0.60 dpa), (e) 13.75×10^{14} ions/cm^2 (1.1 dpa). Lower row: a sequence of SAED patterns of Mu-$8\times8\times8$ ($M1/7$) subjected to 1-MeV Kr^{2+} ion irradiation at 873 K: (f) original, (g) 1.875×10^{14} (0.15 dpa), (h) 3.75×10^{14} (0.29 dpa), (i) 7.5×10^{14} (0.58 dpa), (j) 11.25×10^{14} ions/cm^2 (0.88 dpa). An ion irradiation-induced order-disorder transition occurred in the murataite structure according to the following sequence: murataite superstructure→modulated fluorite structure→disordered fluorite structure. The first disappearance of the weakest satellite spots (long-range ordering) suggests that the long-range order is more sensitive to ion-beam damage than the incommensurate compositional modulation.

ture of the ordered murataite structure disappeared gradually with increasing ion dose, and the ion-beam-induced defect fluorite structure was not stable and became a fully amorphous state above the critical amorphization dose, e.g., ~0.125 dpa (1.56×10^{14} ions/cm^2) for Mu-$5\times5\times5$ in the $M1/7$ sample at room temperature (Fig. 3). The ion irradiation-induced order-disorder transition in the murataite structure can also be observed in the *ex situ* HRTEM images (Fig. 3), as evidenced by the disappearance of the superlattice in the ordered murataite structure. Under initial ion irradiation, the diffraction maxima from the murataite superstructure (long-range order) disappeared first, and materials transformed to a modulated fluorite structure, as revealed by the diffraction patterns [Figs. 6(b) and 6(g)] consist of the diffraction subset of the basic fluorite unit cell and unequally weak satellite diffraction maxima caused by the incommensurate compositional modulations. Continuous ion-beam irradiation caused a redistribution of chemical compositions (incommensurate composition modulations), leading to a disordered fluorite structure [Figs. 6(d) and 6(i)]. These results suggest that the long-range order is more sensitive to ion-beam damage than the incommensurate compositional modulation. The ion irradiation-induced order-disorder transition occurs in murataite structure according to the following sequence: murataite superstructure→modulated fluorite structure→disordered fluorite structure. A thermally induced phase decomposition and the formation of Fe-rich nanocrystals, as a result of the reduction of Fe^{3+} to Fe^{2+} upon thermal treatment in vacuum condition, were observed in murataite leading to the polycrystalline ring in the diffraction patterns [Figs. 6(e) and 6(j)]. The murataite structure remained unchanged after the heat treatment despite of the slight change in chemical compositions due to the Fe-rich phase decomposition. The Fe-rich nanocrystals display a greater radiation resistance than the murataite polytypes, as evidenced by the ring patterns of Figs. 6(e) and 6(j). The details of the thermal-treatment-induced phase decomposition and nanocrystal formation of murataite structure were discussed elsewhere.[30]

Order-disorder transitions play a critical role in the energetics (e.g., defect formation and migration energies), phase stability, and physical and electronic properties of many solid-state systems.[31] There has been much interest in recent years in examining and modeling the process of cation order-disorder transitions, especially in minerals and ceramics in which the cation ordering is an efficient response to variations in temperature and chemical composition.[32] An order-disorder phase transition usually occurs in high-temperature phases showing alternating patterns of long-range correlations; while, in low-temperature phases, atoms are arranged randomly with no long-range correlation. Two cases of cation ordering can be defined as convergent and nonconvergent ordering. In convergent ordering, two or more crystallographic sites become symmetrically equivalent when averaging the site occupancies, and the order-disorder process is associated with a symmetry change. In nonconvergent ordering, the atomic sites cannot become symmetrically equivalent even with the identical occupancies at each site. In this study, we show an ion irradiation-induced order-disorder transition from the murataite structure to the parent-structure-type, a defect fluorite structure. This is similar to the pyrochlore-to-fluorite structural transition, attributed to the cation disordering at A and B sites in the pyrochlore superstructure, $A_2B_2O_7$.[17,18,29] The murataite-to-fluorite structural transition also results from an irradiation-induced disordering of cations among the three specific cation sites in the murataite structure of $A_3B_6C_2O_{22-x/2}$. The murataite superstructure with long-range correlations exists in the as-synthesized samples, as indicated by the weaker superlattice maxima in the diffraction patterns. At the initial stage of

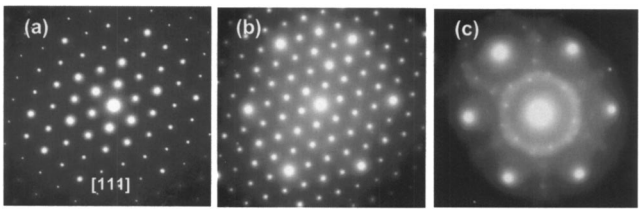

FIG. 7. A sequence of SAED patterns along the [111] zone axis of the disordered murataite structure subjected to 1-MeV Kr^{2+} ion irradiation at 873 K: (a) original, (b) 1.25×10^{14} (0.108 dpa), and (c) 2.5×10^{15} ions/cm^2 (2.16 dpa). Ion-beam-induced fluorite structure is stable with respect to a fully amorphous state.

irradiation, the superlattice maxima in the SAED patterns (Figs. 3 and 6) disappeared first, suggesting the loss of the long-range order. This result indicates that disordering of the long-range correlations dominates at the initial stage of the irradiation. The change in the local chemical composition requires only a few nearest-neighbor exchanges among equivalent sites, leading to the transition from an ordered murataite to a modulated fluorite structure, and this involves a symmetry change. The disordering of atoms with strong atomic scattering coefficients under further ion irradiation, located at planes that intercept at 1/3 of [111] of the large Mu-$5\times5\times5$ or Mu-$8\times8\times8$ unit cells, causes the transition from a modulated fluorite structure to an anion-deficient fluorite structure.

The irradiation at elevated temperature may stabilize the ion-beam-induced defect fluorite structure in murataite, and thus higher ion doses were required to amorphize the defect fluorite structures formed from the murataite structure at a higher temperature. For example, the ion-beam-induced defect fluorite structure can be amorphized at a relatively low dose at room temperature (e.g., ~0.125 dpa for the Mu-$5\times5\times5$ polytype in the $M1/7$ sample); however, it is stable with respect to the fully amorphous state for irradiation temperatures above ~930 and 1030 K for the Mu-$5\times5\times5$ and Mu-$8\times8\times8$ in the $M1/7$ sample, respectively. The ion-beam-induced murataite-to-fluorite structural transition also occurs in disordered murataite. Figure 7 shows a sequence of SAED patterns of disordered murataite (in $M3/7$) at 873 K irradiated by 1-MeV Kr^{2+}. With the increase in ion dose, the relative intensity of diffraction maxima from the basic fluorite unit cell increases. For the disordered murataite, the ion-beam-induced disordered fluorite structure is stable with respect to the amorphous state at a dose of ~2.16 dpa (2.5×10^{15} ions/cm^2) at 873 K. In contrast, for the Mu-$5\times5\times5$ phase ($M1/7$), the ion-beam-induced fluorite structure can be amorphized at a dose of ~1.1 dpa (1.375×10^{15} ions/cm^2) at 873 K (Fig. 6) and is stable upon further ion beam irradiations when the irradiation temperature is above 973 K (Fig. 8). These results suggest that the stability of ion-beam-induced defect fluorite structure in murataite polytypes varies as a function of the extent of structural disorder. A lower temperature is required to stabilize the ion-beam-induced defect structure for compositions with higher degrees of structural disordering, suggesting that the intrinsic structural disordering leads to a greater tendency toward an ion-beam-induced order-disorder structural transition.

C. Effects of the degree of disordering on ion-beam-induced amorphization

Ion-beam-induced amorphization and order-disorder structural transitions have been investigated extensively in the closely associated pyrochlore compositions $A_2B_2O_7$ (A=La to Lu, and Y; B=Ti, Zr, Sn, etc.).[19,29,33–35] The susceptibility of pyrochlore compositions to ion-beam-induced amorphization is strongly correlated with the tendency toward the order-disorder structural transition. Pyrochlore compounds with less deviation from the ideal fluorite structure, as characterized by smaller 48f oxygen x positional parameter, have a greater tendency toward an ion-beam irradiation-induced order-disorder structural transition and energetically prefer the disordered fluorite structure over the amorphous state.[19,33–36] Thus, these pyrochlores have a greater resistance to ion-beam-induced amorphization. The deviation of pyrochlore structure from the ideal fluorite

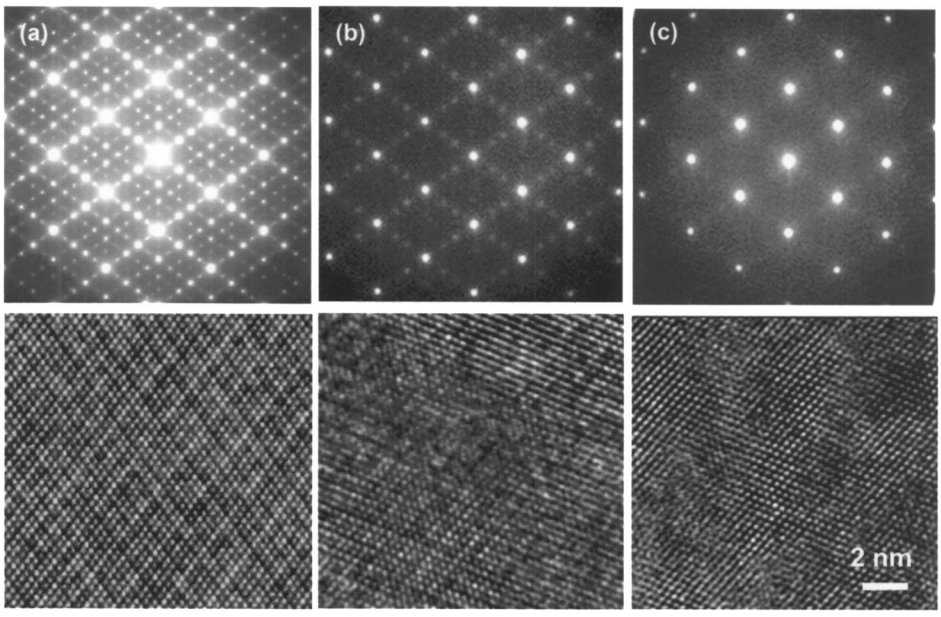

FIG. 8. A sequence of SAED patterns and corresponding HRTEM images of five-multiple murataite ($M1/7$) irradiated by 1-MeV Kr^{2+} at 973 K at a dose of: (a) original, (b) 3.125×10^{14} (0.25 dpa), and (c) 1.25×10^{15} ions/cm^2 (1.0 dpa). The ion-beam-induced fluorite structure was stabilized at elevated irradiation temperature of 973 K. The murataite-to-fluorite transition follows the sequence: murataite superstructure →modulated fluorite structure →disordered fluorite structure.

structure is strongly affected by the cation ionic radius ratio at the *A* and *B* sites, the cation electronic configuration (e.g., bond type), and the degree of structural disorder.[19,29,33–36] However, no direct experimental results have documented the effect of the degree of the structural disorder on ion-beam-induced amorphization and the order-disorder structural transition in fluorite-related phases. In this study, we have shown that there is a more energetically-favored accommodation of a defect fluorite structure upon ion-beam irradiation for the disordered murataite structure, as compared with other murataite polytypes with greater degrees of structural ordering. This suggests an important effect of the degree of intrinsic structural order/disorder on the energetics of the disordering processes, the tendency toward an order-disorder structural transition, and the susceptibility to ion-beam-induced amorphization of fluorite-related compounds. These conclusions are supported by both the critical amorphization temperatures and the stability of ion-beam-induced fluorite structures for disordered murataite and murataite superstructures with high degrees of structural order under the same irradiation conditions.

Variations in degree of ordering result in changes in the free energy, and this affects phase stability. The order-disorder transition is usually associated with the energy difference, $\Delta E = E_{\mathrm{dis}} - E_{\mathrm{ord}}$.[37] A calorimetric study[38] suggested a smaller energy barrier for the order-disorder transition to a completely disordered fluorite from a $Gd_2Zr_2O_7$ pyrochlore with a high degree of structural disordering as compared with a completely ordered pyrochlore superstructure. The influence of structural order/disorder can also be inferred from recent theoretical simulations of pyrochlore compositions, focusing on the energetics of *A*- and *B*-site cation disordering and its effect on oxygen vacancy disorder.[39–41] For $La_2Zr_2O_7$, an increase in the structural disorder (e.g., La–Zr exchange) causes the calculated cation antisite defect energy to be lowered from 2 to 1.5 eV. The experimental results of this study, along with the theoretical simulations, emphasize the correlation between the degree of intrinsic structural order/disorder, the energetics of the order-disorder process, and the susceptibility of fluorite-related compounds to ion-beam-induced amorphization.

IV. CONCLUSIONS

Murataite-structure-types were synthesized with different structural periodicities from disordered murataite to $3\times3\times3$, $5\times5\times5$, and $8\times8\times8$ multiples of the fluorite-type unit cell. The ion-beam-induced murataite-to-defect-fluorite structural transition was observed in synthetic murataite ceramics. The long-range ordering is more sensitive to ion-beam damage than the incommensurate compositional modulations. An increasing tendency toward the order-disorder structural transformations was found in the fluorite-related structures that have a higher degree of structural disordering, as evidenced by the lower critical amorphization temperature and greater stability of ion-beam-induced defect fluorite structure. This study presents the first experimental evidence that confirms the significant effects of intrinsic structural disorder on the energetics of the disordering processes. Thus, the tendency toward an order-disorder structural transition and the susceptibility to ion-beam-induced amorphization for fluorite-related compounds depend, in part, on the initial degree of intrinsic disorder prior to irradiation.

ACKNOWLEDGMENTS

The authors thank the staff of the IVEM-Tandem Facility at the Argonne National Laboratory for assistance during ion irradiation experiments. This work was supported by the Office of Basic Energy Sciences, U.S. DOE under DOE grant (DE-FG02-97ER45656).

[1] J. B. Goodenough, Nature (London) **404**, 821 (2000).
[2] P. K. Moon and H. L. Tuller, Solid State Ionics **28–30**, 470 (1988).
[3] H. L. Tuller, Solid State Ionics **52**, 135 (1992).
[4] Z. Y. Can, H. Narita, J. Mizusaki, and H. Tagawa, Solid State Ionics **79**, 344 (1995).
[5] W. F. Chu, V. Leonhard, H. Erdmann, and M. Ilgenstein, Sens. Actuators B **4**, 321 (1991).
[6] T. Hibino, Y. Kuwahara, T. Otsuka, N. Ishida, and T. Oshima, Solid State Ionics **107**, 217 (1998).
[7] M. Marwood M and C. G. Vayenas, J. Catal. **178**, 429 (1998).
[8] P. J. Gellings and H. J. M. Bouwmeester, Catal. Today **58**, 1 (2000).
[9] J. B. Goodenough and R. N. Castellano, Solid State Chem. **44**, 108 (1982).
[10] P. Li, I. W. Chen, and J. E. Pennerhahn, Phys. Rev. B **48**, 10074 (1993).
[11] H. L. Tuller, J. Phys. Chem. Solids **55**, 1393 (1994).
[12] M. A. Subramanian, G. Aravamudan, and G. V. S. Rao, Prog. Solid State Chem. **15**, 55 (1983).
[13] S. A. Kramer and H. L. Tuller, Solid State Ionics **82**, 15 (1995).
[14] P. K. Moon and H. L. Tuller, Sens. Actuators B **1**, 199 (1990).
[15] B. J. Wuensch, K. W. Eberman, C. Heremans, E. M. Ku, and J. D. Jorgensen, Solid State Ionics **129**, 111 (2000).
[16] J. Lian, L. M. Wang, S. X. Wang, J. Chen, L. A. Boatner, and R. C. Ewing, Phys. Rev. Lett. **87**, 145901 (2001).
[17] J. Lian, L. Wang, J. Chen, K. Sun, R. C. Ewing, J. M. Farmer, and L. A. Boatner, Acta Mater. **51**, 1493 (2003).
[18] S. X. Wang, B. D. Begg, L. M. Wang, R. C. Ewing, W. J. Weber, and K. V. G. Kutty, J. Mater. Res. **14**, 4470 (1999).
[19] J. Lian, X. T. Zu, K. V. G. Kutty, J. Chen, L. M. Wang, and R. C. Ewing, Phys. Rev. B **66**, 054108 (2002).
[20] G. R. Lumpkin, K. L. Smith, and M. G. Blackford, J. Nucl. Mater. **289**, 177 (2001).
[21] T. S. Ercit and F. C. Hawthorne, Can. Mineral. **33**, 1223 (1995).
[22] N. P. Laverov, S. V. Yudintsev, B. I. Omel'yanenko, B. S. Nikonov, and S. V. Stefanovskii, Geology of Ore Deposits **41**, 85 (1999).
[23] N. P. Laverov, S. V. Yudintsev, T. S. Yudintseva, S. V. Stefanovsky, R. C. Ewing, J. Lian, S. Utsunomiya, and L. M. Wang, Geology of Ore Deposits **45**, 423 (2003).
[24] S. V. Yudintsev, S. V. Stefanovskii, O. I. Kir'yanova, J. Lian, and R. Ewing, At. Energy **90**, 487 (2001).
[25] N. P. Laverov, S. V. Yudintsev, S. V. Stefanovsky, J. Lian, and R. C. Ewing, Doklady Earth Sciences **377**, 175 (2001).
[26] O. V. Karimova, N. I. Organova, and V. G. Balakirev, Crystallogr. Rep. **47**, 957 (2002).
[27] P. Buseck, J. Cowley, and L. Eyring, *High Resolution Transmission Electron Microscopy and Associate Techniques* (Oxford University Press, New York, 1988), pp. 340–342.
[28] S. X. Wang, L. M. Wang, and R. C. Ewing, Phys. Rev. B **63**, 024105 (2001).
[29] R. C. Ewing, W. J. Weber, and J. Lian, J. Appl. Phys. **95**, 5949 (2004).
[30] J. Lian, L. M. Wang, R. C. Ewing, S. V. Yudintsev, and S. V. Stefanovsky, J. Mater. Chem. **15**, 709 (2005).
[31] R. M. Hazen and A. Navrotsky, Am. Mineral. **81**, 1021 (1996).
[32] S. A. T. Redfern, in *Transformation Processes in Minerals*, edited by S. A. T. Redfern and M. A. Carpenter, Reviews in Mineralogy and Geochemistry No. 39 (Mineralogical Society of America and Geochemical Society, Washington, 2000), p. 105.
[33] J. Lian, J. Chen, L. M. Wang, R. C. Ewing, J. M. Farmer, L. A. Boatner,

and K. B. Helean, Phys. Rev. B **68**, 134107 (2003).
[34]J. Lian, L. M. Wang, R. G. Haire, K. B. Helean, and R. C. Ewing, Nucl. Instrum. Methods Phys. Res. B **218**, 236 (2004).
[35]J. Lian, R. C. Ewing, L. M. Wang, and K. B. Helean, J. Mater. Res. **19**, 1575 (2004).
[36]K. B. Helean, S. V. Ushakov, C. E. Brown, A. Navrotsky, J. Lian, and R. C. Ewing, J. Solid State Chem. **177**, 1858 (2004).
[37]G. Ceder, A. F. Kohan, M. L. Aydinol, P. D. Tepesch, and A. van der Ven, J. Am. Ceram. Soc. **81**, 517 (1998).
[38]K. B. Helean, B. D. Begg, A. Navrotsky, B. Ebbinghaus, W. J. Webber, and R. C. Ewing, Mater. Res. Soc. Symp. Proc. **663**, 157 (2001).
[39]K. E. Sickafus, L. Minervini, R. W. Grimes, J. A. Valdez, M. Ishimaru, F. Li, K. J. McClellan, and T. Hartmann, Science **289**, 748 (2000).
[40]R. E. Williford, W. J. Weber, R. Devanathan, and J. D. Gale, J. Electroceram. **3**, 409 (1999).
[41]A. Chartier, C. Meis, W. J. Weber, and L. R. Corrales, Phys. Rev. B **65**, 134116 (2002).